

A Comparison of the Reactivity of “Nonequilibrated” and “Equilibrated” V–P–O Catalysts: Structural Evolution, Surface Characterization, and Reactivity in the Selective Oxidation of *n*-Butane and *n*-Pentane

S. Albonetti,* F. Cavani,* F. Trifirò,*¹ P. Venturoli,* G. Calestani,† M. López Granados,‡ and J. L. G. Fierro‡

*Dipartimento di Chimica Industriale e dei Materiali, Viale Risorgimento 4, 40136 Bologna, Italy; †Dipartimento di Chimica Fisica ed Inorganica, Viale Risorgimento 4, 40136 Bologna, Italy; and ‡Instituto de Catálisis y Petroleoquímica, CSIC, Campus UAM, Cantoblanco, 28049 Madrid, Spain

Received March 16, 1995; revised June 26, 1995; accepted December 28, 1995

Changes occurring on thermal treatment of the precursor of vanadium/phosphorus mixed oxide, the industrial catalyst for the oxidation of *n*-butane, were studied. The precursor was mixed with stearic acid, used as an organic binder for pelletization of the powder. The calcination of the precursor leads to a partially oxidized compound, constituted of an amorphous V^{IV}–P mixed oxide and a crystalline hydrated V^V–P–O phase. The calcined compound, when left in a 1% hydrocarbon/air stream for 100 h leads to a “nonequilibrated” catalyst, and after 1000 h to the “equilibrated” catalyst. The catalytic activity of the nonequilibrated and equilibrated catalysts in *n*-butane and *n*-pentane oxidation was studied and compared; the chemical–physical features of the two catalysts were studied by means of XRD, FT-IR, chemical analysis, TGA, XPS, and TPD. Only well crystallized (VO)₂P₂O₇ was detected in the equilibrated catalyst and a homogeneous distribution of surface centers seems to be present on its surface. In the case of nonequilibrated catalyst, a poorly crystallized (VO)₂P₂O₇ is present together with an amorphous V^{IV}–P–O phase and γ -VOPO₄; these phases define a heterogeneous distribution of at least two kind of surface centers. This surface heterogeneity gives rise to a catalyst less selective in *n*-butane oxidation to maleic anhydride and less specific in the conversion of *n*-pentane to phthalic anhydride. © 1996 Academic Press, Inc.

INTRODUCTION

V–P–O based catalysts are known to be efficient in the selective transformation of *n*-butane to maleic anhydride (1–4) and are employed industrially for this reaction in processes developed by several companies (5, 6). Moreover, the same system was found to oxidize *n*-pentane to maleic and phthalic anhydrides (7–11).

The active phase in *n*-butane oxidation, (VO)₂P₂O₇, is prepared via a multistep transformation of a precursor, VOHPO₄·0.5H₂O (5). The precursor can be either transformed into the active phase *in situ* under reaction conditions or calcined *ex situ* in either air or nitrogen and then

treated under reaction conditions. In the latter case, the calcination gives rise to mixtures of amorphous and crystalline V^V and V^{IV} phases, the relative amounts of which are a function of the conditions of treatment (either oxidizing or nonoxidizing) (5).

The nature of the phases present in the catalyst affects remarkably the catalytic behavior in *n*-butane oxidation; this effect has been studied by several authors, and the contemporaneous presence of oxidized V^V–P–O and reduced V^{IV}–P–O phases has been pointed out as a necessary condition in order to have an active and selective catalyst (12–14). The relative amounts of V^V and V^{IV} under reaction conditions is a function of the thermodynamic properties of the solid–gas system represented by the catalyst surface and the reactant mixture, which can be more or less oxidative depending on the relative concentration of the oxygen and the hydrocarbon, on the temperature and pressure employed, and which can accelerate the structural transformations of the catalyst itself. V^V–P–O and V^{IV}–P–O phases exhibit structural similarities that allow, under the reaction conditions, easy redox cycles between different oxidation states of vanadium (15–17). Other factors that affect the catalytic performance are the surface dynamics of the hydrocarbon (18) and of the oxygen (19) species on the catalyst surface. One of the most important aspects is that the structural evolution of the catalyst from the beginning of its lifetime (this has often been referred to as a “nonequilibrated” compound) in the reaction environment finally leads to the structure that is thermodynamically more stable under usual reaction conditions in the equilibrated catalyst (20), i.e., the vanadyl pyrophosphate, which is a V^{IV}–P–O phase, even though this does not exclude the presence of surface V^{III} and V^V species. This aging phenomenon may take several hundred hours, or in some cases shorter times, depending on the reaction conditions and on the structural composition of the nonequilibrated catalyst. The structural changes and the modifications occurring under the reaction conditions are accompanied by modifications in the catalytic performance in *n*-butane oxidation (21–23).

¹ To whom correspondence should be addressed.

The formation of phthalic anhydride from *n*-pentane is a unique property of the V-P-O system; other vanadium-based systems lead only to the formation of maleic anhydride (24). From this point of view, the reaction of *n*-pentane oxidation is a more suitable probe than that of *n*-butane oxidation. In fact, the formation of a wider range of products allows a better characterization of the reactivity of the sites. The production of phthalic anhydride requires not only oxidation sites but also condensation centers in order to obtain a C₈ molecule starting from a C₅ reactant. Therefore the formation of phthalic anhydride must be related to some particular property of the surface structure of V-P mixed oxides which makes this reaction a probe to achieve more information on the surface properties of the V-P-O system. The aim of the research work reported here was to study and compare the bulk properties, reactivity, and surface properties of nonequilibrated and equilibrated V-P-O catalysts in the selective oxidation of *n*-butane and *n*-pentane. The different phases present in these samples, their surface properties, and the comparison of their catalytic activity in both reactions should be useful in clarifying the requirements for the formation of anhydrides on the surface sites.

METHOD

The catalyst was prepared in organic medium by the following procedure. V₂O₅ (15 g) was suspended in 90 ml of isobutyl alcohol and 60 ml of benzyl alcohol. The suspension was stirred continuously under reflux for 3 h, cooled to room temperature, and then 16.2 g of 99% *o*-H₃PO₄ was added. The slurry was heated under reflux with constant stirring for 2 h, cooled, filtered, washed with isobutyl alcohol, and the filtrate was dried at 150°C for 24 h.

XRD patterns were recorded using a computer controlled Philips PW 1050 diffractometer and Cu K α radiation.

FT-IR spectra were recorded at a resolution of 4 cm⁻¹ on a Nicolet 57DX spectrometer with the sample powder diluted with KBr (2%) and pressed into self-supporting wafers.

Chemical analyses were carried out to determine the valence state of vanadium following the usual titration procedure with KMnO₄ for V^{IV} and Mohr salt for V^V (12).

XPS spectra were recorded using a Fisons Escalab MkII spectrometer employing Mg K α radiation (photon energy 1253.6 eV) and an electron take-off angle of 45°. The base pressure of the spectrometer was typically 10⁻⁹ mbar. The X-ray gun was operated at 12 kV and 10 mA, corresponding to a power of 120 W. The O 1s, P 2p, V 2p, and C 1s energy regions were recorded for each sample. Data analysis was carried out using a VGS 5000 data system based on the DEC PDP11 computer. The methodology employed for peak fitting and peak deconvolution was the following: typically

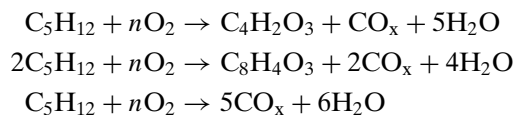
1.8- 2.7-eV linewidths and a Gaussian/Lorentzian mix with a Lorentzian contribution of 30% were employed for the V 2p envelope. Spectra were corrected for sample charging by referencing photoelectron peaks to the C 1s peak at 284.9 eV. Samples were also sputtered in the pretreatment chamber using an Ar⁺ beam of 3 keV and a current density of 120 nA/cm². In the V 2p core level region, the spectra were complicated by the interference of an O 1s peak in the region of the V 2p_{1/2} component. This is due to the contribution of secondary exciting photons (Mg K $\alpha_{3,4}$) present in the non-monochromatic X-ray source.

Thermogravimetric experiments were conducted using a Cahn microbalance connected to a gas handling system. The samples (35 mg) were heated under a flow of 15 cm³/min dry air at a rate of 4°C/min. The microbalance was interfaced with a data station which allowed weight changes to be recorded at intervals of 0.5 min.

TPD tests were carried out as follows. The catalyst samples were first pretreated in flowing dry air (30 cm³/m) at 340°C (heating rate 5°C/min) for 1 h and then cooled down to 300°C and evacuated for 1 h to *P* = 10⁻⁴ mbar. Successively, the temperature was raised to 340°C and 100 Torr of hydrocarbon was kept in contact with the sample for 1 h. The sample was then cooled down and when room temperature was reached evacuation for 1 h was carried out to *P* = 10⁻⁴ mbar. For the TPD tests, the temperature was raised at a rate of 5°C/min to 720°C under vacuum. Several *m/z* fragments were followed, using a quadrupole device connected to the reactor outlet. The most important fragments were CO and CO₂, H₂, O₂ and H₂O.

The catalytic tests were carried out at atmospheric pressure and were performed in a tubular stainless steel flow reactor at atmospheric pressure. The reaction products were collected by bubbling the outlet stream into pure acetone-containing condensers and analyzed on a 1-h-reaction basis; permanent gases were collected by a gas-tight syringe. All products were analyzed by means of Hewlett-Packard 5890 II gas chromatography, equipped with FID and TCD. Carbon oxides and oxygen were separated and analyzed by means of a packed Carbosieve S column, with oven temperature programmed from 40 to 240°C. Condensable products and unreacted hydrocarbons were separated and analyzed in a 0.53 mm OV-17 column, with the oven temperature programmed from 80 to 200°C.

Three grams of catalyst was used for catalytic tests, sieved into particles with size ranging from 0.3 to 0.5 mm. The usual experimental conditions for catalytic tests were the following: *n*-pentane, 1 mol% in air; *n*-butane, 1.7 mol% in air; temperature, 340°C; W/F, 3 g s/ml. Yields were calculated according to the following equations:



$$\begin{aligned} \text{Yield\% to maleic anhydride (MA)} &= \\ & (\text{mol MA produced}) \times 100 / (\text{mol } n\text{-C}_5\text{H}_{12} \text{ fed}) \\ \text{Yield\% to phthalic anhydride (PA)} &= \\ & (\text{mol PA produced}) \times 2 \times 100 / (\text{mol } n\text{-C}_5\text{H}_{12} \text{ fed}) \\ \text{Yield\% to carbon oxides (CO}_x) &= \\ & \{(\text{mol CO}_x \text{ produced}/5) - (\text{mol MA produced}) - 2(\text{mol} \\ & \text{PA produced})\} 100 / (\text{mol } n\text{-C}_5\text{H}_{12} \text{ fed}). \end{aligned}$$

Carbon oxides which are considered in the calculation of the yield to CO_x are therefore only those produced by complete overoxidation, while those formed as coproducts in the formation of maleic and phthalic anhydrides are not taken into account.

RESULTS

Thermal Evolution of the Precursor in Air

Thermal changes in the pellets. The catalyst precursor, $\text{VOHPO}_4 \cdot 0.5\text{H}_2\text{O}$, was prepared according to the “anhydrous” procedure in an organic medium (5); details of the preparation are given under Method. Before the calcination and activation procedures, the precursor powder was mixed with 5 wt% stearic acid, which is necessary for easy tableting of the powder. Cylindrical pellets (200 g) were then calcined at 380°C for 5 h. The X-ray pattern of the sample after this treatment is displayed in Fig. 1a (patterns of compounds in Figs. 1b and 1c will be discussed later), while its FT-IR spectrum is given in Fig. 2a. Other features of this sample are listed in Table 1; the average oxidation degree of vanadium (4.40) indicates the presence of both V^{V} and V^{IV} phases. The absence of reflections relative to any known V^{IV} crystalline phase in the XRD pattern suggests that an amorphous phase holds the V^{IV} . The surface area is $11 \text{ m}^2/\text{g}$, remarkably lower than the one typical of the vanadyl pyrophosphate (usually, in the range 20 to $30 \text{ m}^2/\text{g}$). Neither the XRD pattern nor the FT-IR spectrum show the features typical of the $(\text{VO})_2\text{P}_2\text{O}_7$. These results were unexpected; in fact, it is known that a dehydration in air of the precursor prepared in organic medium usually leads to a compound in which the prevailing phase is the vanadyl pyrophosphate, though often it is of low crystallinity and mixed with a V^{5+} phase, and that in order to achieve such a wide extent of vanadium oxidation it is necessary to carry out the calcination at temperatures higher than 450°C .

Thermal changes in the powder. In order to evaluate whether the observed phenomena were due to the use of the precursor shaped in the form of pellets, we carried out a study of the changes in the precursor in the form of powder, but mixed with stearic acid. Figure 3 shows the *ex situ* XRD pattern (samples kept under room atmosphere) of the samples after increasing periods of elapsed time at 380°C . The reflections from the hemihydrate vanadyl orthophosphate progressively disappear (none are left after 1 h), with an evident contemporaneous amorphization and subsequent

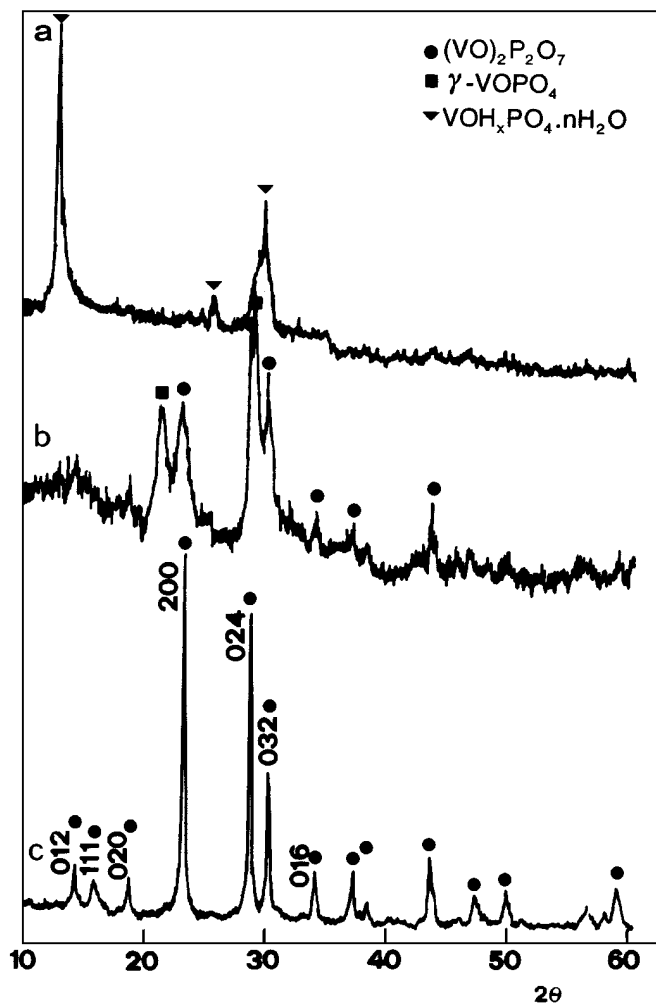


FIG. 1. XRD patterns of the precursor mixed with stearic acid and calcined at 380°C . (a) Calcined catalyst; (b) nonequilibrated catalyst; (c) equilibrated catalyst.

formation of the $(\text{VO})_2\text{P}_2\text{O}_7$ phase. Broadening of the $(h00)$ reflections indicates that the sample is not well crystallized. Leaving the sample for 5 h leads to the appearance of the same reflections also observed in the case of the sample in Fig. 1a; however, this phase becomes the prevailing one with respect to the vanadyl pyrophosphate only for very long periods of calcination (60 h). On the contrary, in the case of the calcination carried out with a large amount of catalyst shaped in pellets (Fig. 1a) this phase was formed after a few hours; therefore, in this case a mass effect was clearly present, which accelerated the formation of this phase.

The effect of stearic acid addition was confirmed by examining the structural evolution of the precursor powder at 380°C when this was not preliminarily mixed with the stearic acid (Fig. 4). The two following effects are observed: (i) the disappearance of the reflections of the hemihydrate vanadyl orthophosphate is completed in a longer period of time than with the mixed precursor; (ii) only the reflections

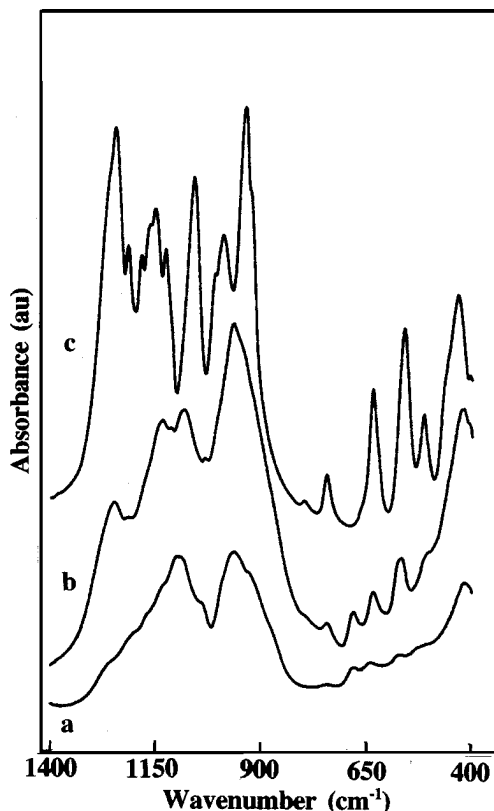


FIG. 2. FT-IR spectra of (a) the calcined sample, (b) the nonequilibrated catalyst, and (c) the equilibrated catalyst.

which developed after 10 h of calcination at 380°C correspond to those of a poorly crystallized vanadyl pyrophosphate; also an amorphous phase seems to be present. No other crystalline phase was obtained even after 30 h of calcination. The reflections relative to the crystalline phase displayed in Fig. 1a were formed only after calcination at 450°C for 20 h at least (Fig. 5a). Therefore, the presence of stearic acid accelerates the structural transformations and also lowers the temperature at which they occur. It is likely that the combustion of the stearic acid locally increases the effective temperatures; with large amounts of catalyst shaped in pellets the release of the heat is less efficient, probably causing a marked increase in the local temperature.

TABLE 1

Valence State as Determined by Chemical Analysis and BET Surface Area of Samples

Sample	Vanadium average oxidation state	Surface area (m^2/g)
Calcined	4.40	11
Nonequilibrated	4.36	11
Equilibrated	≤ 4.00	23

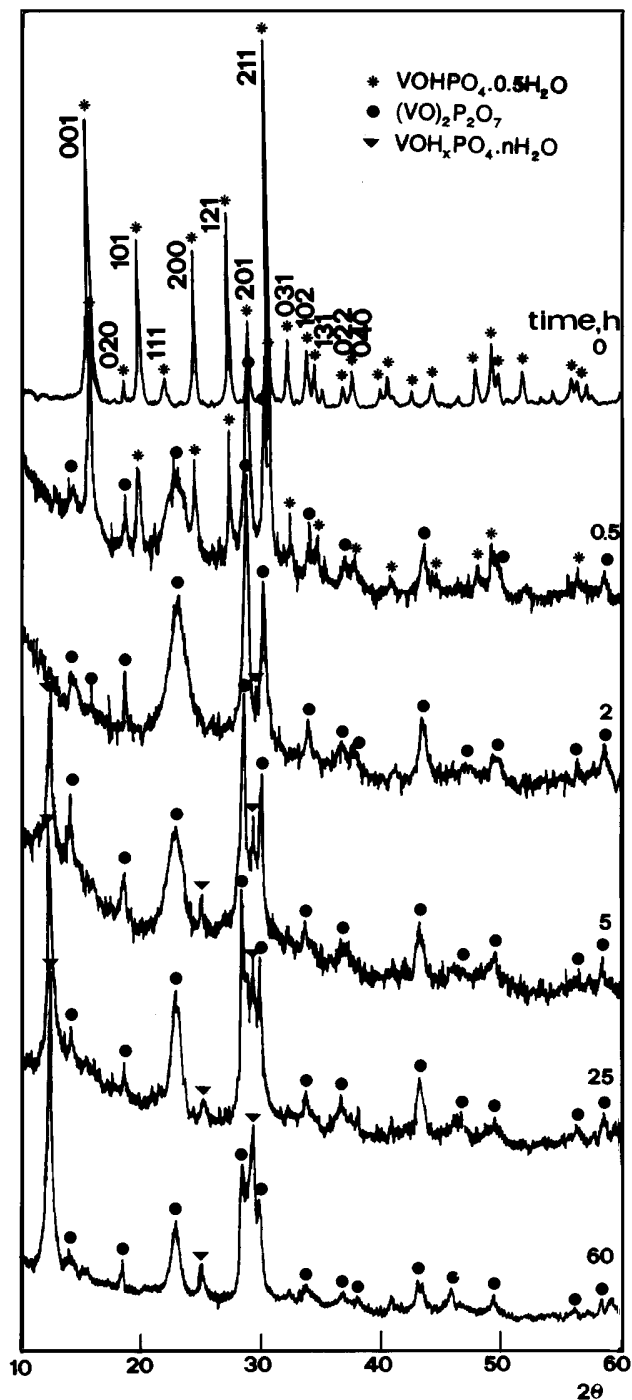


FIG. 3. XRD patterns of the precursor mixed with 5 wt% stearic acid and calcined at 380°C for increasing periods of time.

Figure 5b shows the pattern of the unmixed precursor when the latter is stored at room temperature in dry air after calcination at 450°C ; when the sample was left at room atmosphere for some days, the spectrum displayed in Fig. 5a was restored. Therefore it seems that the two compounds whose patterns are shown in Fig. 5 are in a hydration–dehydration equilibrium.

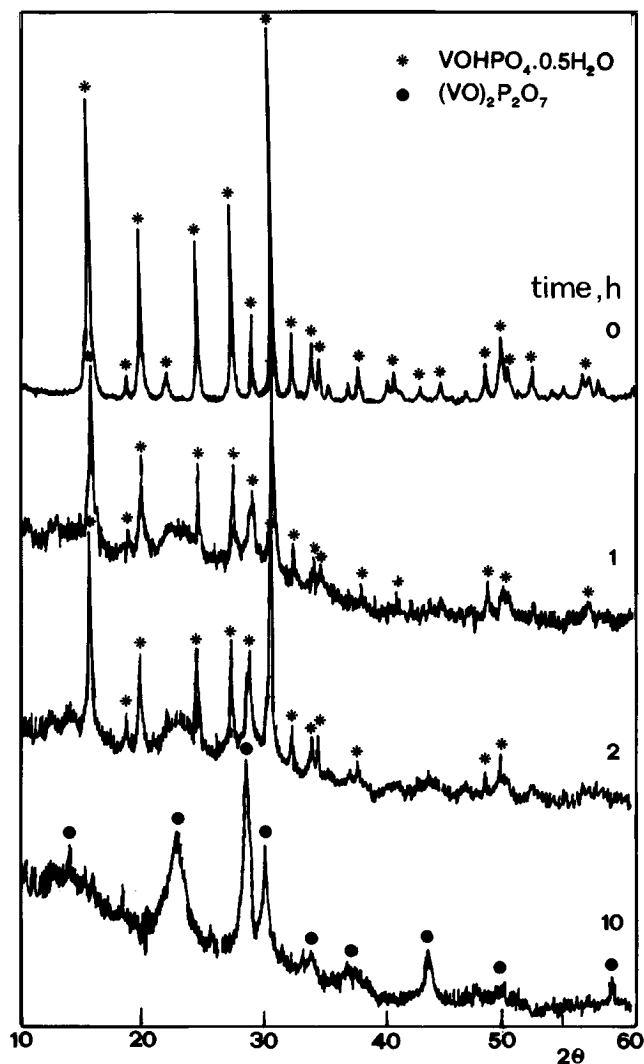


FIG. 4. XRD patterns of the precursor not mixed with stearic acid and calcined at 380°C for increasing periods of time.

Structural Evolution of the Calcined Compound in the Reaction Environment

Reported in Figs. 1b and 1c are the *ex situ* XRD patterns of samples used for catalytic tests; after unloading, the samples were stored under room atmosphere. In particular, Fig. 1b shows the pattern of the “calcined” sample (whose pattern is given in Fig. 1a) after approximately 100 h time-on-stream in *n*-pentane oxidation; hereinafter this sample is referred to as nonequilibrated catalyst. It is worth mentioning that the biggest variations in the catalytic performance are observed within the first 100 h time-on-stream, while after this period the behavior, even though not definitely constant, is much more stable. The pattern exhibits diffraction lines assignable to poorly crystallized $(\text{VO})_2\text{P}_2\text{O}_7$; most of the sample must be amorphous as indicated by the low signal-to-noise ratio; in addition, there

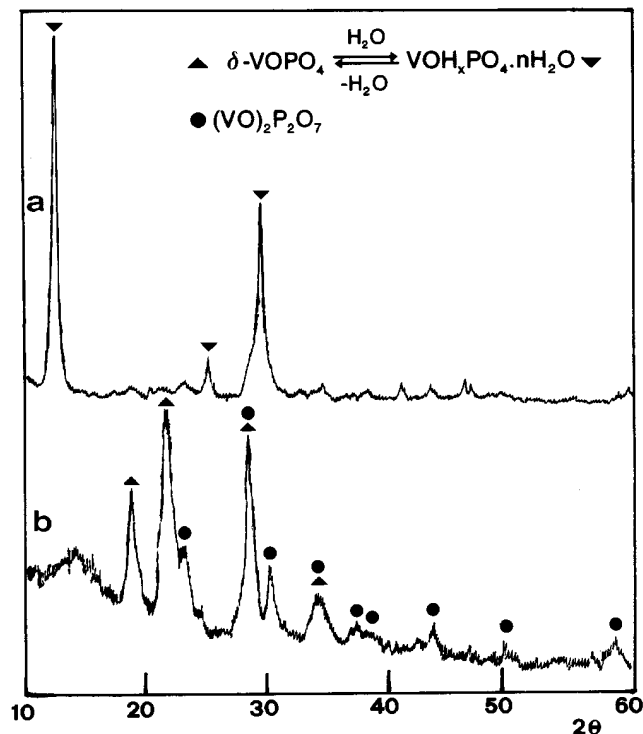


FIG. 5. XRD patterns of the precursor calcined at 450°C for 20 h and stored under either (a) room atmosphere or (b) anhydrous conditions.

are two main reflections at $d = 4.17 \text{ \AA}$ and at $d = 3.10 \text{ \AA}$; the assignment of these peaks is uncertain. They might be attributed to the (004) and (040) reflections, respectively, of $\gamma\text{-VOPO}_4$, which are reported to be very intense in the reference compound (15, 17) (even though other very intense reflections typical of this phase are lacking in our spectrum, for instance the one at $d = 4.90 \text{ \AA}$). Indeed, intense peaks at around $d = 3.10 \text{ \AA}$ are reported for all VOPO_4 phases, and this makes a definite attribution a hard task.

The XRD pattern in Fig. 1c is obtained after 1000 h under reaction conditions. This catalyst will be referred to as equilibrated catalyst. The pattern agrees very well with that of well crystallized $(\text{VO})_2\text{P}_2\text{O}_7$ (25).

Figure 2 reports the IR spectra of the nonequilibrated (Fig. 2b) and equilibrated (Fig. 2c) catalysts. The spectrum of nonequilibrated sample is quite complicated; some bands can be attributed to $(\text{VO})_2\text{P}_2\text{O}_7$, but other bands are present, which confirm the contemporaneous presence of other phases. A clear attribution to a specific phase is impossible. The FT-IR spectrum for equilibrated catalyst is typical of $(\text{VO})_2\text{P}_2\text{O}_7$ (1, 12).

Table 1 gives the average valence state of the vanadium, as determined by chemical analysis and the values of specific surface area. The nonequilibrated catalyst is only slightly more reduced (average degree of oxidation, 4.36) than the calcined catalyst. Therefore, under the reaction atmosphere

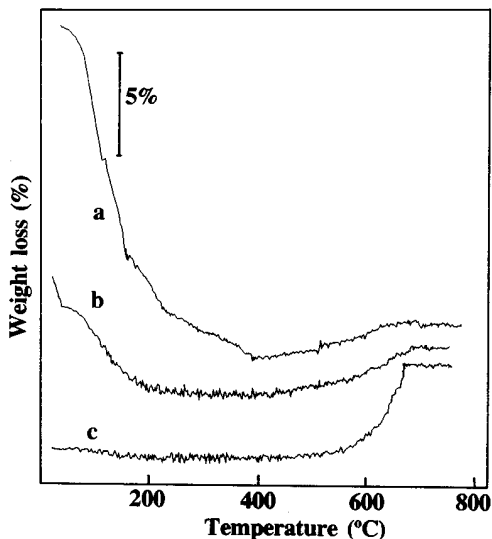


FIG. 6. Weight changes in air at increasing temperatures for (a) the calcined sample, (b) the nonequilibrated catalyst, and (c) the equilibrated catalyst.

the reduction of vanadium is a very slow process, slower than the transformation of the amorphous $V^{IV}/P/O$ phase into crystalline $(VO)_2P_2O_7$. It is not unlikely that some amorphous phase is still left as indicated by the XRD pattern. The "equilibrated" sample is instead completely reduced, at least within the sensitivity limits of the method employed for the determination of the valence state. The surface area of the calcined sample is $11 \text{ m}^2/\text{g}$; after 100 h time-on-stream (nonequilibrated sample) the surface area remains substantially unaltered. The surface area of equilibrated sample is about $23 \text{ m}^2/\text{g}$.

Thermogravimetric tests were carried out on the calcined sample, and for nonequilibrated and equilibrated catalysts. The results are reported in Fig. 6. The weight loss at below 400°C can be ascribed to a dehydration process. This weight loss for the nonequilibrated sample (Fig. 6b) is much lower than for the calcined sample (Fig. 6a). The equilibrated sample (Fig. 6c) does not lose weight at all, which agrees with the bulk characterization; in fact, only $(VO)_2P_2O_7$ was detected in this sample. The weight gain at above 400°C can be assigned to the oxidation of V^{IV} phases to $V^V OPO_4$ phases. The weight increase of the equilibrated sample is much higher than that for the other two samples, in agreement with the results of the chemical analysis, which indicated a lower average oxidation degree for the equilibrated catalyst. Another observation concerns the onset temperature for the oxidation of vanadium, which is the highest in the equilibrated catalyst. This confirms that the well crystallized $(VO)_2P_2O_7$ is oxidized with more difficulty than the amorphous or poorly crystallized V^{IV} phase present in the calcined sample and in the nonequilibrated catalyst, respectively.

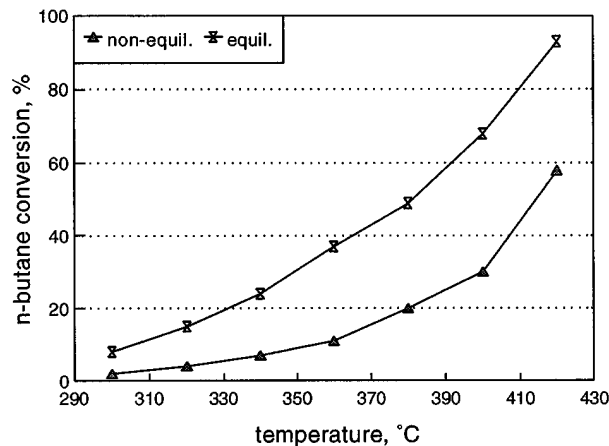


FIG. 7. *n*-Butane conversion as a function of the reaction temperature over nonequilibrated and equilibrated catalysts. Reaction conditions: 1.7 mol% *n*-butane in air, W/F 3 g/ml.

Comparison between Nonequilibrated and Equilibrated Catalysts in Paraffin Oxidation

Reactivity in *n*-butane oxidation. Reported in Figs. 7 and 8 are the *n*-butane conversion as a function of reaction temperature and the selectivity vs conversion plot, respectively, for the two samples. The equilibrated catalyst displays a higher activity than the nonequilibrated one; the higher activity can be justified by the higher surface area; however, the areal activity (activity per unit surface area) is still higher for the equilibrated catalyst. The apparent activation energy for the nonequilibrated catalyst is 20.5 kcal/mol and for the equilibrated catalyst is 18.5 kcal/mol .

The selectivity dependence upon conversion is very different for the two samples. For the nonequilibrated catalyst the selectivity to maleic anhydride is lower (around 50%), and is fairly constant over the entire range of temperatures examined, whereas the equilibrated catalyst exhibits an ini-

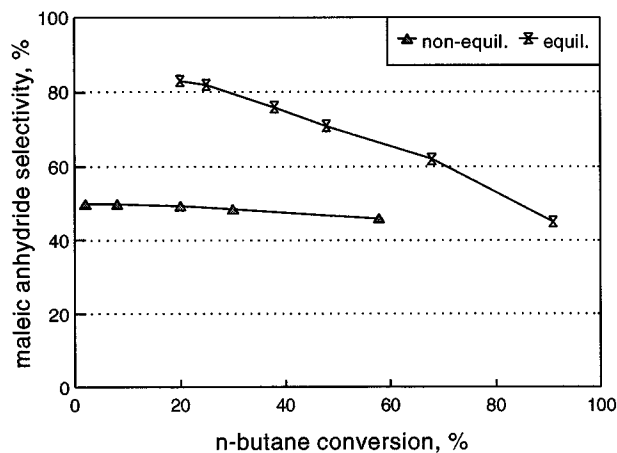


FIG. 8. Selectivity to maleic anhydride as a function of the *n*-butane conversion; conditions as in Fig. 7.

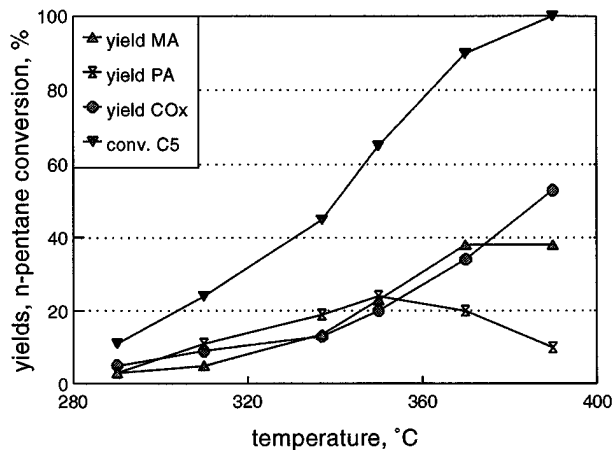


FIG. 9. *n*-Pentane conversion and yields as functions of the reaction temperature on equilibrated catalyst. Reaction conditions: 1% *n*-pentane in air, W/F 3 g s/ml.

tially higher selectivity (higher than 80%), which then decreases as the *n*-butane conversion increases. This occurs even though the operating temperatures are lower than that of the nonequilibrated catalyst. The decrease, therefore, can not be attributed to the reaction conditions, but rather may well reflect a different reaction network. A fairly constant selectivity with conversion means the presence of two parallel reactions (one selective to maleic anhydride, the second one unselective) which are characterized by approximately comparable apparent activation energies. In the case of the equilibrated sample the selectivity, extrapolated to zero conversion, is very high, suggesting that at low temperature the surface sites are highly selective to the formation of maleic anhydride and that on increasing the temperature the formation of CO_x is preferred.

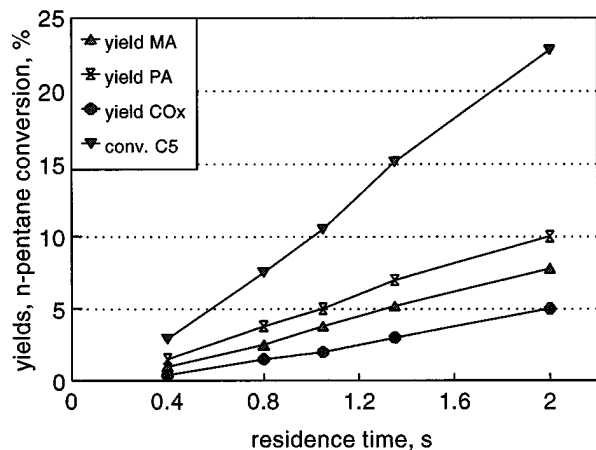


FIG. 10. *n*-Pentane conversion and yields as functions of the residence time on equilibrated catalyst. Reaction conditions: 0.46% *n*-pentane in air, temperature, 315°C.

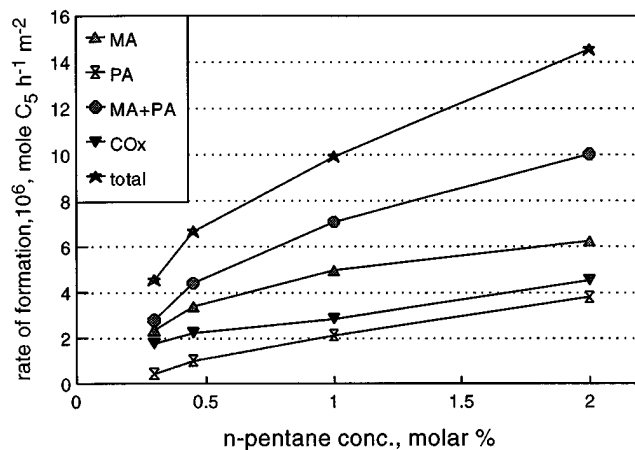


FIG. 11. Rates of formation of the products and of *n*-pentane depletion as functions of the *n*-pentane concentration in feed on nonequilibrated catalyst. Reaction conditions: O₂ 20%; temperature, 340°C; W/F 3 g s/ml.

Reactivity in n-pentane oxidation. Reported in Fig. 9 are the effects of the reaction temperature on the *n*-pentane conversion and product yields for the equilibrated catalyst. The yield in maleic anhydride increases over the range of temperatures examined, leveling at 370°C; phthalic anhydride instead reaches a maximum at 350°C and then decreases, with a corresponding enhancement in CO_x formation. The effect of residence time is reported in Fig. 10 at 315°C. The trend of the yields is typical of parallel reactions: the maleic and phthalic anhydrides are formed through independent pathways, and at this temperature the two products are stable.

The rates of *n*-pentane depletion (expressed with respect to the specific surface area) and product formation as a function of *n*-pentane concentration for the two samples are reported in Figs. 11 and 12, while the trends of the selectivities

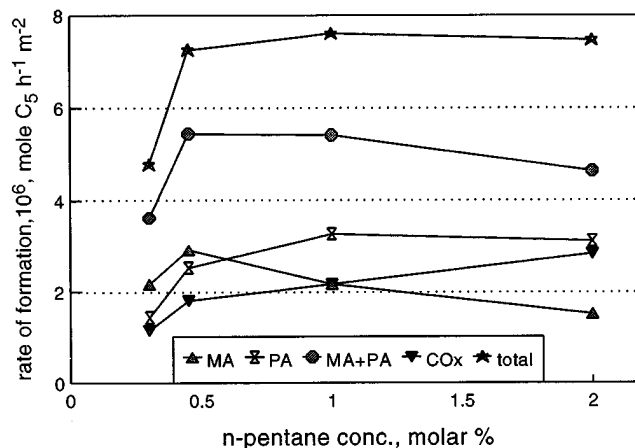


FIG. 12. Rates of formation of the products and of *n*-pentane depletion as functions of the *n*-pentane concentration in feed on equilibrated catalyst. Reaction conditions as in Fig. 11.

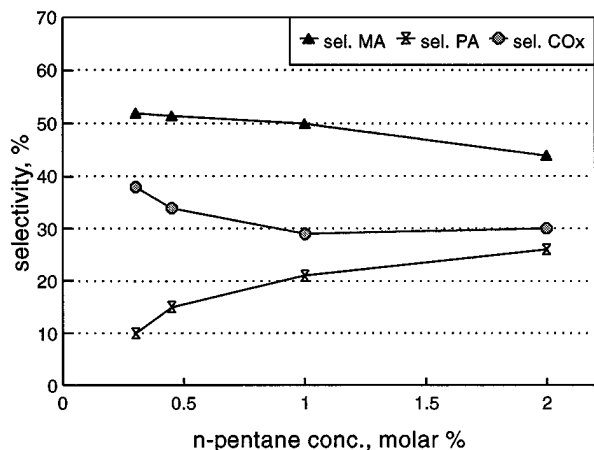


FIG. 13. Selectivity to the products as a function of the *n*-pentane conversion on nonequilibrated catalyst. Reaction conditions as in Fig. 11.

are shown in Figs. 13 and 14. The relative order of activity depends on the level of *n*-pentane concentration at which the two catalysts are compared. The rates of product formation reach a "plateau" at low hydrocarbon concentration for the equilibrated sample (Fig. 12), indicating saturation of the surface sites. The nonequilibrated catalyst, in contrast, exhibits a continuous increase in the rates of product formation, and reaches a higher value than the equilibrated sample at high *n*-pentane concentration (Fig. 11). In both samples an increase in *n*-pentane concentration leads to an increase in the phthalic to-maleic anhydride ratio; however, in the equilibrated sample this increase is much more marked.

Figure 15 compares the yield to anhydrides from the two paraffins. In the equilibrated catalyst the amount of maleic anhydride from *n*-butane is the same as the amount of anhydrides (phthalic plus maleic) from *n*-pentane (thus in-

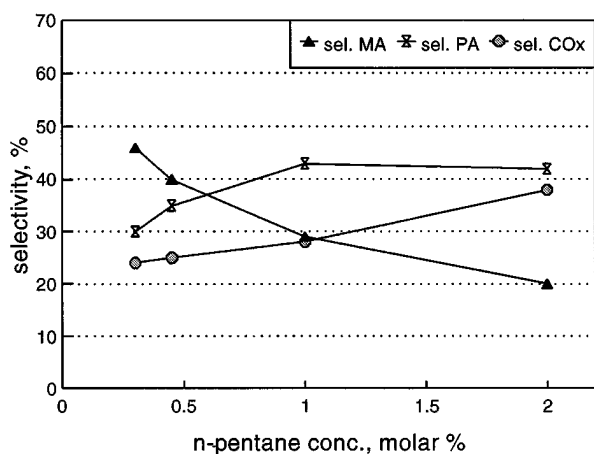


FIG. 14. Selectivity to the products as a function of the *n*-pentane conversion on equilibrated catalyst. Reaction conditions as in Fig. 11.

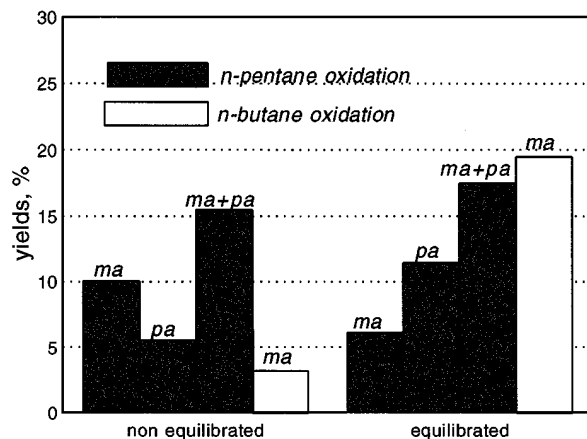


FIG. 15. Yields to maleic anhydride (ma) and to phthalic anhydride (pa) from *n*-butane and *n*-pentane on nonequilibrated and equilibrated catalysts. Reaction conditions: 1.7% hydrocarbon in air; temperature, 340°C; W/F 3 g/s/ml.

dicating that the same active sites are involved in the two reactions), while in the nonequilibrated catalyst the overall amount of anhydride from *n*-pentane is far higher than the maleic anhydride from *n*-butane.

Comparison between Nonequilibrated and Equilibrated Catalysts in Surface Properties

XPS characterization. The results of XPS analysis for the three samples are summarized in Table 2. Reference spectra for $\text{VOHPO}_4 \cdot 0.5\text{H}_2\text{O}$ (where vanadium is V^{IV}) and for $\text{VOPO}_4 \cdot 2\text{H}_2\text{O}$ (a V^{V} phase), were also studied; Fig. 16 reports the spectra for the reference compounds and for the three samples. The spectrum of the calcined sample confirms the presence of both V^{IV} and V^{V} . The signal at BE 518 eV corresponds well to that of the $\text{V } 2p_{3/2}$ in the

TABLE 2
Binding Energies (eV) of Core Electrons and XPS Intensity Ratios of the Samples (Evacuated at 20°C) and of Reference Compounds (Evacuated at 100°C) in the V 2p Region

Sample	O 1s	P 2p	V 2p _{3/2}
Calcined	531.3 (70)	133.6	516.9 (50)
	532.6 (30)		518.2 (50)
Nonequilibrated	531.3 (70)	133.7	516.9 (50)
	532.6 (30)		518.2 (50)
Equilibrated	531.3 (75)	133.7	517.0 (100)
	532.5 (25)		
Precursor, $\text{VOHPO}_4 \cdot 0.5\text{H}_2\text{O}$	531.2 (73)	132.7	516.8 (100)
	532.6 (38)		
$\text{VOPO}_4 \cdot 2\text{H}_2\text{O}$	531.2 (73)	132.4	518.1 (100)
	532.1 (27)		

Note. Figures in brackets indicate the approximate percentage ($\pm 10\%$) of each signal as detected by peak deconvolution.

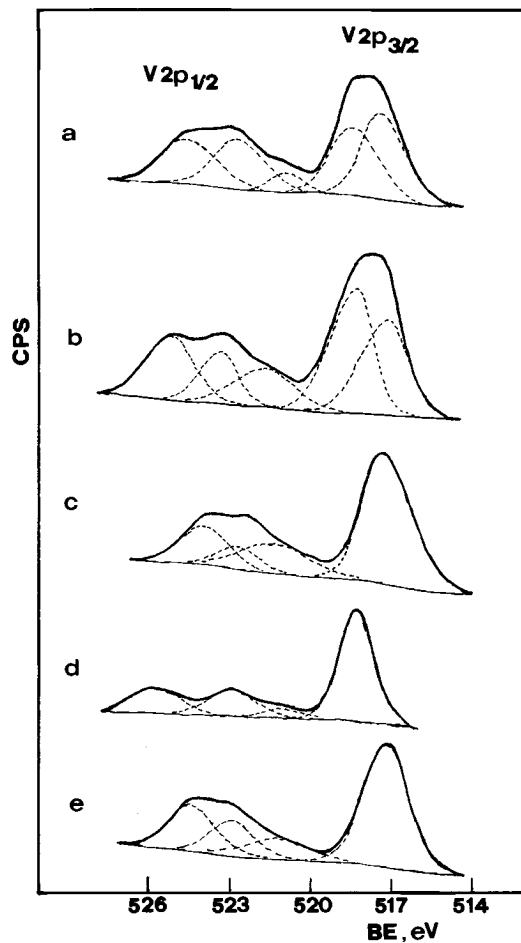


FIG. 16. XPS spectra of (a) the "calcined" sample, (b) the nonequilibrated catalyst (c) the equilibrated catalyst (d) the reference compound VOPO₄·2H₂O, and (e) the precursor VOHPO₄·0.5H₂O.

reference V^V phase. The spectrum of the nonequilibrated catalyst shows the presence of V^V at the surface, together with V^{IV}, while the spectrum of the equilibrated catalyst shows only the signal relative to the V^{IV}. It is worth noting that the V^{IV} on the surface of the samples cannot arise from the evacuation treatment which the samples undergo before the XPS spectra are recorded: VOPO₄·2H₂O does not exhibit any V^{IV} signal even when evacuated at 100°C.

TPD characterization. When the *n*-pentane and *n*-butane interacted with the catalyst surface at 340°C several products were detected when the temperature was increased above room temperature under vacuum. CO, CO₂, H₂O, H₂, and O₂ were the main fragments detected. Fragments with *m/z* values assignable to hydrocarbons were also seen but the intensity of these signals was much less (around 1000 times weaker). CO and CO₂ were the most intense fragments with C atoms and they were chosen as probes for describing the hydrocarbon interaction with the surface. TPD signals for CO and CO₂ as a function of

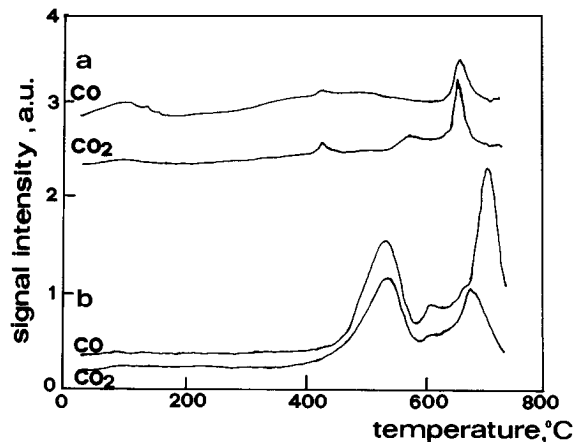


FIG. 17. TPD spectra of CO and CO₂ on nonequilibrated catalyst after adsorption of (a) *n*-butane and (b) *n*-pentane.

temperature for the catalysts are represented in Figs. 17 and 18.

In the case of the equilibrated sample (Fig. 18), CO and CO₂ were released mainly at high temperatures. Moreover, the behavior from *n*-butane and *n*-pentane was very similar in terms of the temperature at which the CO_x desorption occurred and of the amount of released CO_x. Completely different was the case for the nonequilibrated catalyst (Fig. 17). Thus, the overall amount of CO_x desorbed when the *n*-butane was first adsorbed was smaller than the amount arising from *n*-pentane adsorption. Moreover, in the case of *n*-pentane, CO and CO₂ desorbed in two temperature

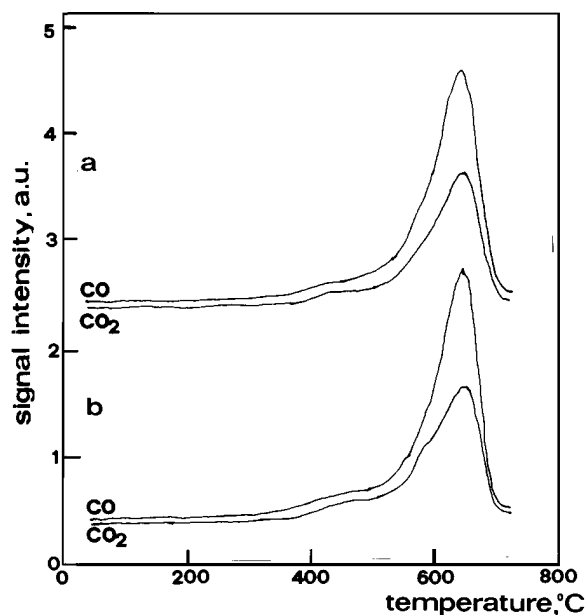


FIG. 18. TPD spectra of CO and CO₂ on equilibrated catalyst after adsorption of (a) *n*-butane and (b) *n*-pentane.

ranges; the amount of desorbed CO_x at low temperature was similar to that desorbed at high temperatures.

DISCUSSION

Structural Evolution in Air of the Precursor When Mixed with Organic Binders

The active phase in *n*-butane and *n*-pentane oxidation, $(\text{VO})_2\text{P}_2\text{O}_7$, can be formed either through the direct transformation of the precursor, $\text{VOHPO}_4 \cdot 0.5\text{H}_2\text{O}$, inside the reactor in the reaction environment, or by first dehydrating the precursor by calcination in air or in nitrogen, and then aging the catalyst inside the reactor (4, 5). The heating of the precursor in air, when the latter is prepared in an organic medium and contains a slight excess of phosphorus, first leads to the dehydration of the $\text{VOHPO}_4 \cdot 0.5\text{H}_2\text{O}$ (at temperatures ranging from 330 to 380°C), with development of an amorphous compound, which is then transformed into a poorly crystallized $(\text{VO})_2\text{P}_2\text{O}_7$, the active phase in *n*-butane oxidation (5, 12). The complete crystallization of the vanadyl pyrophosphate takes several hundreds of hours to be completed in the reaction environment (20). Initially, it was hypothesized that the transformation of the precursor to the vanadyl pyrophosphate was a topotactic reaction, thus occurring very quickly and with only a small structural rearrangement (26, 27). However, even though the two crystalline structures have structural similarities, the formation of the crystalline $(\text{VO})_2\text{P}_2\text{O}_7$ is not so easy, at least when a precursor of lower crystallinity (as is the case for those prepared in organic medium) is used.

The assignment of all reflections shown in Fig. 1a (whose pattern is the same as the one displayed in Fig. 5a and is also observed in Fig. 3) is rather difficult. Three main reflections are observed: the most intense is at $d = 7.12 \text{ \AA}$, and two less intense ones appear at $d = 3.55$ and 3.04 \AA ; this compound is obtained either by calcination of the pellets at 380°C (Fig. 1a), or by calcination of the pure powder at 450°C at least (Fig. 5a), or is formed together with the vanadyl pyrophosphate after prolonged calcination of the powder mixed with the stearic acid at 380°C (Fig. 3). In addition, patterns in Fig. 5 indicate that this phase is hydrated and can be reversibly dehydrated yielding the sample in Fig. 5b; this is also confirmed by thermogravimetric tests, which indicate a considerable weight loss for the calcined sample. Tetragonal $\text{VOPO}_4 \cdot 2\text{H}_2\text{O}$ is characterized by a diffraction peak at $d = 7.45 \text{ \AA}$, attributed to the (001) reflection (17, 28), which is shifted toward lower *d*-spacings (7.3 \AA) by progressive removal of water molecules (29); this peak is reported by some authors as the most intense peak (29), by others as a weak peak (17). Other reflections typical of this compound are found at $d = 4.75$, 3.10 , and 1.55 \AA . Therefore, the pattern shown in Figs. 1a, 3, and 5a cannot be assigned to $\text{VOPO}_4 \cdot 2\text{H}_2\text{O}$. A pattern similar to that one here

reported has been reported by Schneider (30), by Harrouch Batis *et al.* (13) after catalytic tests with $\text{VOPO}_4 \cdot 2\text{H}_2\text{O}$, by Moser (31) for V-P-O catalysts prepared by spray drying at high temperature and by Miquel and Katz (29) for samples prepared by flame hydrolysis. These authors attributed the pattern to $\text{VOH}_x\text{PO}_4 \cdot y\text{H}_2\text{O}$ (according to Schneider (30) a $\text{VOH}_{0.16}\text{PO}_4 \cdot 1.9 \text{ H}_2\text{O}$ phase, with $\text{V}^{4.84+}$, formed during reduction of the $\text{VOPO}_4 \cdot 2\text{H}_2\text{O}$), even though the reflection at $d = 3.04 \text{ \AA}$ (observed in our case, and also reported by Miquel and Katz (29)) does not match with any other known V-P-O phase. Several VOPO_4 phases possess reflections close to this (15, 17): $\gamma\text{-VOPO}_4$ at $d = 3.06 \text{ \AA}$, $\beta\text{-VOPO}_4$ at $d = 3.07 \text{ \AA}$, $\alpha_{\text{II}}\text{-VOPO}_4$ at $d = 3.06 \text{ \AA}$; however, in all cases the other major reflections of each of these phases are not observed in our spectrum. A possible attribution of the reflections at $d = 3.55 \text{ \AA}$ and $d = 3.04 \text{ \AA}$ is to the (101) and (111) planes of $\alpha_{\text{II}}\text{-VOPO}_4$; however, in this case, too, the other very intense reflection typical of this compound, at $d = 4.42 \text{ \AA}$, is not observed in our spectrum. In addition, patterns in Fig. 5 clearly indicate that these reflections belong to a hydrated phase rather than to a simple VOPO_4 ; this hydrated phase can be reversibly dehydrated, giving the compound whose pattern is shown in Fig. 5b. Recently, Ben Abdelouahab *et al.* (32), reported that all VOPO_4 phases, with the exception of $\beta\text{-VOPO}_4$, can be reversibly hydrated, leading to the formation of $\text{VOPO}_4 \cdot 2\text{H}_2\text{O}$. To sum up, we prefer to assign the observed pattern to $\text{VOH}_{0.16}\text{PO}_4 \cdot 1.9\text{H}_2\text{O}$.

The spectrum in Fig. 5b shows intense reflections at $2\theta = 18.8^\circ$, 21.6° , 22.9° , 27.9° , 30.0° , and 34.1° , plus some less intense peaks at higher values of 2θ . Some of these reflections might correspond to the most intense ones of the $\delta\text{-VOPO}_4$ (15, 17) (which shows peaks at $2\theta = 19.6^\circ$, 22.1° , 24.2° , 28.6° , 30.3° , 34.8°), even though all corresponding peaks in Fig. 5b are shifted with respect to these values. Other reflections correspond well to those of the vanadyl pyrophosphate, also present in Fig. 5a.

The transformation of the precursor when it is calcined in air is shown in Fig. 3 (for the powder mixed with stearic acid) and in Fig. 4 (for the pure powder of precursor). The changes in the patterns shown in Fig. 3 indicate that the destruction of the $\text{VOHPO}_4 \cdot 0.5\text{H}_2\text{O}$ generates a product which is in part amorphous, and in part constituted of poorly crystallized vanadyl pyrophosphate. The significant enlargement of the reflection at approximately $2\theta = 23^\circ$ can be assigned either to the contemporaneous formation of a δ - or a γ - VOPO_4 phase (which are characterized by intense reflections in this position), as indicated by other authors (33), or by assuming particular structural or morphological features of the vanadyl pyrophosphate along the corresponding (200) crystallographic plane. This latter hypothesis seems to us more likely, due to the following considerations: (i) the other intense reflections of γ - and $\delta\text{-VOPO}_4$ are absent in the spectrum; (ii) it is known that

many factors, such as the nature of the precursor and the procedure employed for the dehydration, can remarkably affect the morphology and the crystallinity of the corresponding vanadyl pyrophosphate (i.e., in the absence of V^V in the compound) and that these aspects mainly condition the shape of the reflection relative to the (200) crystallographic plane. This reflection can be either very intense and narrow, or very broad (12, 34–36), depending, for instance, on the development of the basal (100) face. Recently, Thompson *et al.* (37, 38) have been confuting the importance attributed to broadening of the (200) reflection; the authors reported that this effect does not depend on vanadium disorder, as initially stated (12), but rather might be due to more subtle variations in the position of oxygen atoms; indeed, it was reported that this reflection is invariant with respect to “linear disorder” effects in the structure, such as columnar disorder of the metal atoms.

Finally, Fig. 3 shows that after 5 h of calcination, also the oxidized hydrated phase discussed above is formed in the sample mixed with stearic acid; the same does not occur with the pure, unmixed precursor (Fig. 4). Therefore, the data indicate that the presence of large amounts of organic compounds can remarkably affect the structural evolution of the precursor in air; it is likely that the burning of these compounds (such as that of the binder necessary to allow tableting of the powder for fixed-bed applications) causes a local overheating and leads to the formation of V^V -P-O phases whose formation would otherwise need much higher temperatures (at least 450°C, as shown in Fig. 5); in addition, all the structural transformations (destruction of the precursor and production of the intermediate amorphous phase to the vanadyl pyrophosphate) are accelerated.

Transformation of the Calcined Compound in the Reaction Environment

When the fresh catalyst is loaded in the reactor (after precursor dehydration) and left in the reaction environment, the poorly crystallized compound is slowly transformed into crystalline $(VO)_2P_2O_7$. The structural evolutions occurring during these transformations lead to variations in the catalytic performance, as also described by Sola *et al.* (22), by Kubias *et al.* (21), and by Zhang-Lin *et al.* (14, 23). It has been claimed that reaching a steady catalytic performance and a stable catalytic composition and structure (equilibrated catalyst) can take from a few hundred hours to more than 1000 h (20). The time necessary to complete this transformation is a function of the reaction conditions employed (temperature, pressure, hydrocarbon-to-oxygen ratio) and of the physico-chemical features of the fresh catalyst.

The results reported here indicate that when the starting compound is highly oxidized, a long period of aging is needed for catalyst equilibration. The XRD pattern of the nonequilibrated sample (after 100 h time-on-stream)

shows the reflections relative to a poorly crystallized $(VO)_2P_2O_7$ and of a V^V -P-O which we can, with some uncertainty, indicate as a γ - $VOPO_4$. The calcined sample, instead, shows reflections relative only to the hydrated, oxidized phase, which we have suggested corresponds to $VOH_{0.16}PO_4 \cdot 1.9H_2O$ (29, 30).

During aging, the following transformations occur:

(1) Dehydration of the $VOH_{0.16}PO_4 \cdot 1.9H_2O$ compound, with formation of γ - $VOPO_4$: this is in agreement with indications given by other authors (32).

(2) Reduction of V^V to V^{IV} : this is a slow reaction, as indicated by the fact that after 100 h time-on-stream the average oxidation degree is only slightly changed, from 4.40 to 4.36. It has to be considered that under our experimental conditions (1–2% hydrocarbon in air, thus with a large excess of oxygen with respect to the stoichiometric requirement) the gas phase probably possesses a rather weak reducing power.

(3) Crystallization of amorphous V^{IV}/P oxide into $(VO)_2P_2O_7$: the comparison of FT-IR spectra and XRD patterns of the calcined and nonequilibrated samples show clear evidence of this evolution; however, the crystallinity of the vanadyl pyrophosphate is still poor, and some amount of an amorphous phase is present. This transformation occurs without any significant variation in the surface area, which remains approximately 11 m²/g.

The complete reduction of the vanadium and crystallization of the vanadyl pyrophosphate need much longer times; the equilibrated catalyst only possesses V^{IV} , as indicated by both XPS and chemical analysis (even though the presence of small amounts of V^V on the catalyst surface cannot be excluded), only exhibits the XRD reflections and IR spectrum typical of crystalline $(VO)_2P_2O_7$, and possesses a surface area of 23 m²/g.

Correlation between Catalytic Activity and Bulk/Surface Features

The structural and surface differences between the equilibrated and the nonequilibrated catalysts also correspond to differences in catalytic behavior in both *n*-butane and *n*-pentane oxidation. The correlation between the catalytic performance and the chemical-physical features indicates the following:

(1) The **equilibrated catalyst** is more active in the oxidation of *n*-butane. This higher activity can be attributed to its higher specific surface area, even though the areal activity (that referred to the surface area) is higher than that of the nonequilibrated catalyst. It possesses surface sites that are specific in the oxidation of the *n*-butane to maleic anhydride (at low temperature the selectivity is very high), so yielding the desired product with a higher selectivity.

Different is the case for the *n*-pentane oxidation. The two catalysts possess a comparable activity at low hydro-

carbon concentration; however, the equilibrated catalyst does not increase further the rate of product formation when the hydrocarbon concentration is increased above 0.5 mol% (Fig. 12), while the nonequilibrated one shows a continuous increase in the rate of *n*-pentane conversion (Fig. 11). This indicates that the equilibrated catalyst possesses a lower number of surface active sites per unit surface area. However, these sites are specific for the conversion of *n*-pentane to phthalic anhydride (Fig. 14); in fact, this catalyst yields the highest phthalic-to-maleic anhydride ratio under all conditions.

Significantly, the productivity to maleic anhydride from *n*-butane is the same as that to anhydrides (maleic plus phthalic) from *n*-pentane (see Fig. 15). These results suggest the existence of a single type of active center on the catalytic surface, which is able to activate both hydrocarbons and therefore point to a homogeneous surface. The two anhydrides form through two parallel pathways (Fig. 10); this indicates that the conversion of activated *n*-pentane either to the maleic or to the phthalic anhydride is not a function of the nature of the active site, but is likely to be due to other factors, such as the way the paraffin has been adsorbed and activated and the probability of finding other activated molecules in the surrounding area.

(2) The **nonequilibrated catalyst** is less active in *n*-butane oxidation and less specific in the formation of maleic anhydride. It has surface centers which are not saturated at high *n*-pentane concentration (Fig. 11), indicating the presence of higher number of surface sites which are able to activate the *n*-pentane. These sites are less specific to phthalic anhydride (the phthalic-to-maleic ratio is lower than that of the equilibrated sample) (Fig. 13), even though the overall selectivity to the anhydrides is higher than in equilibrated catalyst (80% against 70%). With *n*-pentane the yield in anhydrides is higher than the yield in maleic anhydride from *n*-butane (see Fig. 15). The phthalic-to-maleic ratio also increases with increasing *n*-pentane concentration, but the formation of maleic anhydride is always preferred to that of phthalic anhydride.

The different behavior in *n*-butane and *n*-pentane oxidation indicates that the surface of this catalyst discriminates between the interaction with the two hydrocarbons; in other words, the surface possesses at least two kinds of sites (or ensembles of active sites): these are (i) sites that convert *n*-butane to maleic anhydride and which are also active in the transformation of *n*-pentane to both anhydrides, more preferentially to maleic anhydride, and (ii) other sites which are inactive in *n*-butane oxidation but are able to oxidize *n*-pentane to the anhydrides, with higher selectivity to the maleic anhydride. This justifies the observed behavior: the slightly lower specific activity of the nonequilibrated catalyst in *n*-butane oxidation, and the higher activity in *n*-pentane oxidation, especially at high hydrocarbon concentration.

The TPD results are in agreement with the catalytic results. The surface of the equilibrated catalyst is homogeneous: there is only one type of site able to interact with both hydrocarbons. In the case of nonequilibrated catalyst, instead, the amount of *n*-butane activated and desorbed in the form of CO_x is very low, much lower than the amount formed from *n*-pentane interaction. Moreover, the nonequilibrated surface is heterogeneous from the point of view of *n*-pentane interaction since the hydrocarbon is released as CO_x in two distinct temperature ranges.

This heterogeneity of surface centers corresponds to a structural heterogeneity; the nonequilibrated sample is characterized by the presence of two crystalline phases at least, namely poorly crystallized (VO)₂P₂O₇ and VOPO₄ (likely to be γ-VOPO₄), while the equilibrated catalyst only possesses well crystallized (VO)₂P₂O₇.

A further indication arising from the data reported is that the conditions necessary to obtain a good catalyst for *n*-butane and *n*-pentane oxidation are different; the (VO)₂P₂O₇ is the most active and selective phase in the *n*-butane oxidation, while the nonequilibrated catalyst is active and selective in the oxidation of the *n*-pentane. However, as the (VO)₂P₂O₇ is more specific to the oxidation of *n*-pentane to the phthalic anhydride, it is likely that the presence of the crystalline vanadyl pyrophosphate guarantees the geometric constraints necessary to direct the activated *n*-pentane along the pathway leading to phthalic anhydride.

ACKNOWLEDGMENT

This work was carried out within the framework of the Human Capital Mobility Fund (EEC), contract CHRX-CT92-0065.

REFERENCES

- Centi, G., Trifirò, F., Ebner, J. R., and Franchetti, V. M., *Chem. Rev.* **88**, 55 (1988).
- Cavani, F., and Trifirò, F., in "Catalysis" Vol. 11, p. 246. Royal Society of Chemistry, Cambridge, UK, 1994.
- See the monograph on "Vanadyl Pyrophosphate Catalyst," *Catal. Today*, (G. Centi, Ed.), **16**, (1993).
- Cavani, F., and Trifirò, F., *Chemtech* **24**, 18 (1994).
- Cavani, F., and Trifirò, F., in "Preparation of Catalysts VI" (G. Poncelet, J. Martens, B. Delmon, P. A. Jacobs, and P. Grange, Eds.), p. 1. Elsevier, Amsterdam, 1995.
- Hodnett, B. K., *Catal. Rev. Sci. Eng.* **27**(3), 373 (1985).
- Centi, G., and Trifirò, F., in "Catalytic Science and Technology" (S. Yoshida, N. Takezawa, and T. Ono, Eds.), Vol. 1, p. 225. Kodansha, Tokyo, 1991.
- Centi, G., Lopez Nieto, J., Pinelli, D., and Trifirò, F., *Ind. Eng. Chem. Res.* **28**, 400 (1989).
- Honicke, D., Griesbaum, K., Augenstein, R., and Yang, Y., *Chem. Ing. Tech.* **59**, 222 (1987).
- Trifirò, F., *Catal. Today* **16**, 91 (1993).
- Braks, D., and Honicke, D., Proceedings of the DGMK Conference on "Selective Oxidations in Petrochemistry" (M. Baerns and J. Weitkamp, Eds.), p. 37, 1992.

12. Busca, G., Cavani, F., Centi, G., and Trifirò, F., *J. Catal.* **99**, 400 (1986).
13. Harrouch Batis, N., Batis, H., Ghorbel, A., Védrine, J. C., and Volta, J. C., *J. Catal.* **128**, 248 (1991).
14. Zhang-Lin, Y., Forissier, M., Sneedeen, R. P., Védrine, J. C., and Volta, J. C., *J. Catal.* **145**, 256 (1994).
15. Ben Abdelouahab, F., Olier, R., Guilhaume, N., Lefebvre, F., and Volta, J. C., *J. Catal.* **134**, 151 (1992).
16. Bordes, E., *Catal. Today* **16**, 27 (1993).
17. Bordes, E., *Catal. Today* **1**, 499 (1987).
18. Busca, G., and Centi, G., *J. Amer. Chem. Soc.* **111**, 46 (1989).
19. Agaskar, P. A., DeCaul, L., and Grasselli, R. K., *Catal. Lett.* **23**, 339 (1994).
20. Ebner, J. R., and Thompson, M. R., *Catal. Today* **16**, 51 (1993).
21. Kubias, B., Rodemerck, U., Wolf, G. U., and Meisel, M., Proceedings on the DGMK Conference on "Selective Oxidations in Petrochemistry" (M. Baerns and J. Weitkamp, Eds.), p. 303, 1992.
22. Sola, G. A., Pierini, B. T., and Petunchi, J. O., *Catal. Today* **15**, 537 (1992).
23. Zhang-Lin, Y., Forissier, M., Védrine, J. C., and Volta, J. C., *J. Catal.* **145**, 267 (1994).
24. Michalagos, P. M., Kung, M. C., Jahan, I., and Kung, H. H., *J. Catal.* **140**, 226 (1993).
25. Linde, S. A., Gorbunova, Yu. E., Lavrov, A. V., and Kuznetsov, V. G., *Dokl. Akad. Nauk SSSR* **245**, 584 (1979).
26. Bordes, E., Johnson, J. W., and Courtine, P., *J. Solid State Chem.* **53**, 270 (1984).
27. Bordes, E., Johnson, J. W., Raminosoma, A., and Courtine, P., *Mater. Sci. Monogr.* **28B**, 887 (1985).
28. Ladwig, G., *Z. Anorg. Allg. Chem.* **338**, 266 (1965).
29. Miquel, P. F., and Katz, J. L., *J. Mater. Res.* **9**(3), 746 (1994).
30. Schneider, A., Thesis, Univ. Bordeaux, 1987.
31. Moser, W. R., in "Catalytic Selective Oxidation" (S. T. Oyama and J. W. Hightower, Eds.), ACS Symp. Series 523, p. 244, Washington, 1993.
32. Ben Abdelouahab, F., Volta, J. C., and Olier, R., *J. Catal.* **148**, 334 (1994).
33. Hutchings, G. J., Desmartin-Chomel, A., Olier, R., and Volta, J. C., *Nature* **368**, 41 (1994).
34. Cornaglia, L. M., Caspani, C., and Lombardo, E. A., *Appl. Catal.* **74**, 15 (1991).
35. Sananes, M. T., Tuel, A., Hutchings, G. J., and Volta, J. C., *J. Catal.* **148**, 399 (1994).
36. Matsuura, I., and Yamazaki, Y., in "New Developments in Selective Oxidation" (G. Centi and F. Trifirò Eds.), p. 563. Elsevier, Amsterdam, 1990.
37. Thompson, M. R., Hess, A. C., Nicholas, J. B., White, J. C., Anchell, J., and Ebner, J. R., in "New Developments in Selective Oxidation II" (V. Cortes Corberan and S. Vic Bellon, Eds.), p. 167, Elsevier, Amsterdam, 1994.
38. Thompson, M. R., private communication.